JOURNAL OF GEOPHYSICAL RESEARCH, VOL. 99, NO. A2, PAGES 2387–2401, FEBRUARY 1, 1994

Tail lobe ion composition at energies of 0.1 to 16 keV/*e*: Evidence for mass-dependent density gradients

O. W. Lennartsson

Lockheed Missiles and Space Company, Incorporated, Research and Development, Palo Alto, California

Abstract. A large set of energetic (0.1- to 16-keV/*e*) ion composition data from the central magnetotail, obtained by the ISEE 1 spacecraft between 10 and $23R_E$ from Earth, is sorted according to measured total ion beta value, in order to investigate whether bulk properties of different ions vary in different ways between plasma sheet and lobes, as suggested by a comparison of certain experimental and theoretical results in the literature. Despite inevitable difficulties with extracting statistically valid data at very low beta (10^{-2} or lower), the results seem to support a recent theoretical model suggesting that lighter ions have a steeper density gradient than heavier ions, especially when comparing H^+ ions with O^+ ions. The results also indicate that ion velocity distributions are fairly isotropic even at low beta, at least those of H^+ ions, although field-aligned flows are common. The results are evaluated in the context of plasma transport and are found to lend some support to the notion that tail lobe convection may be directed inward from the dawn and dusk flanks.

1. Introduction

As far as plasma measurements are concerned, the tail lobe regions of Earth's magnetosphere are unique in that they are typically not identified by characteristic particle signatures but rather by the disappearance of instrument response, or "plasma dropout" [e.g. *Hones et al.*, 1986]. What is known points to a very low particle density, at least inside of a few tens of Earth radii, where 10^{-2} cm^{-3} may be a typical number [*Akasofu et al.*, 1973; *Zwickl et al.*, 1984], and energies significantly lower than in the plasma sheet [*Akasofu et al.*, 1973; *Hardy et al.*, 1979]. It is also known that the lobes contain narrowly collimated tailward streams of ions, at least part of the time, and that these streams consist not only of H^+ ions but to an even greater extent of O^+ ions, presumably of terrestrial origin [*Sharp et al.*, 1981]. The data on these streams are so far the only information available on the ionic composition of the tail lobe plasma.

This study is an extension of the work by *Sharp et al.* [1981], using a much larger data set from the same experiment (on ISEE 1) and taking a different approach. It is motivated by some apparent discrepancies between different sets of tail ion composition data and between data and theory. The difference in the data refers to the studies by *Sharp et al.* [1981] and *Lennartsson and Shelley* [1986]. As already mentioned, the former study found the O^+ ions to be more abundant than H^+ ions in the tail lobes, at least when the geomagnetic 3-hour range index *Kp* is above 3+, whereas the latter study found the H^+ ions to be the usually most abundant in the central plasma sheet, even during geomagnetically disturbed conditions. Nevertheless, by sorting data according to the geocentric solar magnetospheric (GSM) *Z* coordinate (south-north direction), Lennartsson and Shelley found the O^+/H^+ density ratio to peak in a $5R_E$ wide bin centered at $Z = 0$, on average (their Figure 9b), in apparent disagreement with the greater O^+/H^+ ratio in the lobes. This may imply either that the lobe and plasma sheet ions have substantially different origins, or that the use of a fixed-scale coordinate like the GSM *Z* can give misleading results. It is certainly possible that a statistical peak in the O^+/H^+ ratio near $Z = 0$ is mainly the result of spatial thinning of the plasma sheet during substorms [*Hones et al.*, 1971], when the O^+/H^+ ratio is typically enhanced in both the lobes and the plasma sheet.

The difference between data and theory refers to the study by *Lennartsson and Shelley* [1986] and a recent theory of tail pressure equilibria by *Kiessling and Ziegler* [1989]. The latter, which uses statistical mechanics rather than MHD, is the first theoretical analysis of tail equilibria with two ion components present, namely H^+ and O^+ ions. Under fairly general assumptions about the relative bulk velocities of the two ion components and the electrons (affecting the cross-tail current) this theory requires that the O^+ ions form a spatially thicker sheet, in GSM *Z*, than do the H^+ ions (Figures 4 through 7 in that paper). As a consequence, the O^+/H^+ density ratio becomes larger than one in the tail lobes, even if it is much less than one in the central plasma sheet. This may seem to be in agreement with the result of *Sharp et al.* [1981], even though the theoretical velocity distributions are essentially isotropic, not narrow streams, but it is again in apparent disagreement with the statistical *Z* dependence found by *Lennartsson and Shelley* [1986]. Since the theory assumes that each ion component has identical thermal velocity distributions in the plasma sheet and the lobes, except for the overall amplitudes, it suggests that a variation of the O^+/H^+ ratio with *Z* can be due to local conditions rather than to the particle sources. The implication is, as stated by Kiessling and Ziegler, that the effect is produced by the different ionic mass of the two components.

This study, like the one by *Lennartsson and Shelley* [1986], treats the ion data in a statistical fashion, but it sorts them according to the calculated ion beta, instead of GSM *Z*, and follows them well into the lobes. This procedure, as it

Paper number 93JA03201.
0148-0227/94/93JA-03201$05.00

happens, removes the aforementioned discrepancies. The approach differs from that of *Sharp et al.* [1981] in that all detector counts are included here (corrected for background noise), not merely isolated counts exceeding three standard deviations of a Poisson distribution (at least 10 counts per unit sampling). The deficiency in individual counts is compensated for by summing them (weighted) into ion velocity moments, while keeping score of the resulting total standard deviations. The objective is to extract the maximum possible information from available data. The rationale may be described by a metaphor: if anything is hidden in a dark place, one is more likely to see it by going there with only a candle at hand than by staying under the bright porch light.

2. Database

The ion data are from the Plasma Composition Experiment on the ISEE 1 spacecraft [*Shelley et al.*, 1978] and cover for the most part the energy range between 100 eV/e and 16 keV/e. This instrument measures ions at various mass per charge (M/Q) in a cyclic fashion, usually by scanning the full range of energy per charge (E/Q) while maintaining a fixed M/Q. Each E/Q setting is typically kept fixed for at least one full spacecraft spin period (3 s). A complete energy-mass scan cycle in the magnetospheric modes of operation usually requires about 8 to 17 min and includes an M/Q setting (<1) which provides direct measurements of detector noise due to penetrating high-energy radiation (mostly MeV electrons). This detector background is subtracted from the other measurements before converting counts to velocity moments. The ion data are supplemented with magnetic field data from the ISEE 1 flux gate magnetometer [*Russell*, 1978]. A more detailed description of the instrument and the data format is given in the appendix.

The data set has been spatially limited to a "central tail" region, defined according to Figure 1 in terms of GSM coordinates. Each point in Figure 1 represents a single energy-mass scan cycle of the instrument, that is a single mass-resolved plasma sample. This region lies at GSM R between 10 and $23R_E$, the latter being the ISEE 1 apogee, and at $X < -5R_E$ and $-10R_E < Y < 10R_E$. The bias toward positive Z is a consequence of the ISEE 1 orbit. The data span a total time period from January 2, 1978, to March 1, 1980.

The GSM boundaries are somewhat arbitrary, although they encompass a region where the ISEE 1 spacecraft provides regular sampling of the tail lobes (mostly of the northern lobe). Outside of this region, at $|Y| > 10R_E$, the plasma sheet is often too thick (in the Z direction) to allow that, especially during geomagnetically quiet periods. The ISEE 1 is expected to be well inside of the magnetopause while in this region, but the data have been additionally screened for possible evidence of magnetosheath or solar wind plasmas by the data analysis program. This screening has been based on velocity moments, combining the mass-resolved H^+ and He^{++} moments as well as the "total ion" moments, assuming that the latter are well representative of H^+ ions (see appendix).

Apart from the GSM boundaries in Figure 1, the data have not been ordered explicitly by spatial coordinates here. Instead, they have been ordered by the relative strengths of the measured particle and magnetic field pressures perpendicular to the magnetic field vector, that is by the measured ion beta value in the 0.1- to 16-keV/e energy range, or strictly speaking, by an approximate estimate of the true beta. This estimate has been made with the second set of assumptions listed in the appendix (section A2), and always includes the H^+ pressure, and in most cases the partial pressures of He^{++}, He^+, and O^+ ions as well (all four species usually measured).

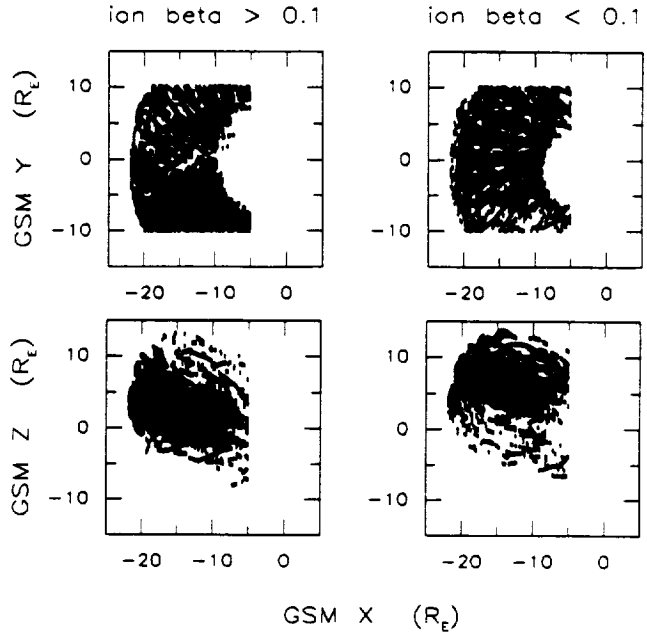

Figure 1. Spatial extent of selected tail data set in geocentric solar magnetospheric (GSM) coordinates, subdivided according to measured ion beta.

This beta value is one obtained in the frame of reference of the spacecraft, rather than the more physically correct value that would be inferred by an observer moving with the local **E** × **B** drift, which is not known. A rough estimate of the resulting error can be made by subtracting, from each partial ion pressure, an energy density corresponding to the trans-B component of the respective drift velocity derived with the first set of assumptions listed in the appendix (section A2). That has been tried and found to have no significant effect on the statistical picture, mainly because that component of the drift energies is relatively small in most cases.

The final size of this data set is further limited by the availability of magnetic tape records of the auroral electrojet (AE) indices, which have been used to divide the data according to geomagnetic activity (see *Kamei and Maeda* [1981] and subsequent data books). As a result, no data from 1977 have been included.

3. Statistical Results

Many aspects of the data are qualitatively similar for different ion species, so in order to save figure space, a single species, namely the H^+, will serve as an example to be referred to later. The H^+ has always been measured here, and it is almost always present in statistically significant numbers.

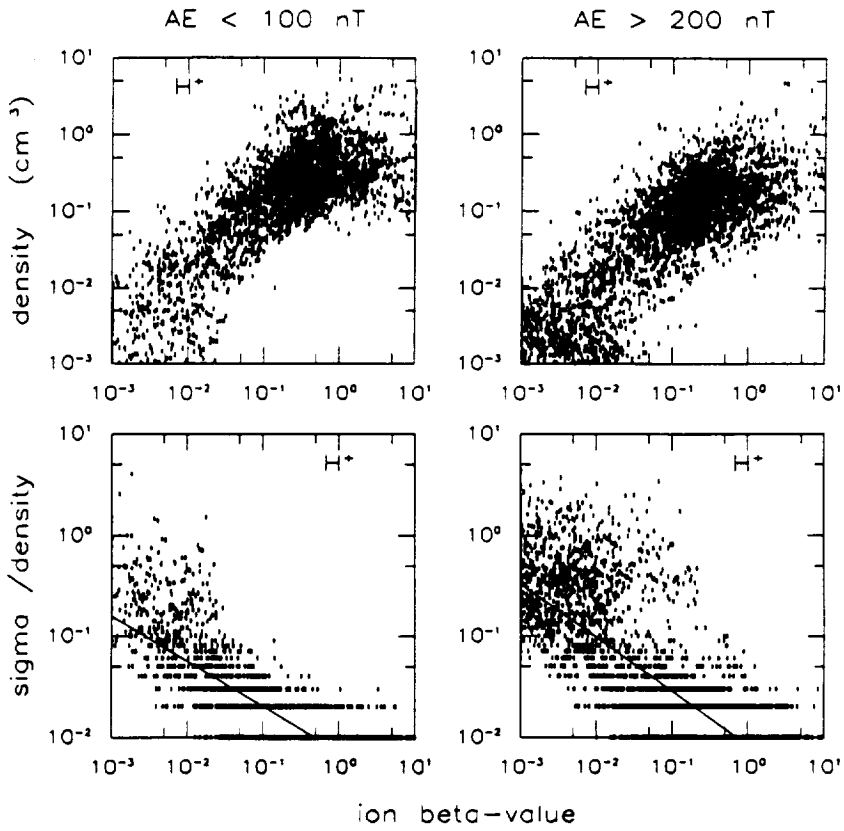

Figure 2. (Top) Density samplings of H^+ ions during (left) quiet and (right) active geomagnetic conditions (see text), and (bottom) statistical uncertainty of each sampling, ordered by corresponding total ion beta. Straight lines intersecting this and following figures are linear least squares fits referred to in the text (all fits are unweighted).

3.1. Proton Density and Energy in Central Tail

Figure 2 shows the H^+ number density (top) in the central tail (Figure 1) and the relative statistical uncertainty (one standard deviation) of this density (bottom), ordered by total ion beta, as defined above, and by geomagnetic activity. The latter has been measured each time by two consecutive hourly *AE* values, one from the preceding hour and one from the current hour (in universal time). In the left panels are only included those H^+ densities obtained when the two *AE* values were both below 100 nT, in the right panels are densities obtained when the two *AE* values were both above 200 nT. This selection does exclude a substantial portion of the data (about 34%), but the differences between quiet and active times are hardly sufficient to justify a third and intermediate group. The reason for using both the preceding and current hours for the *AE* is to allow for some inertia in the transport of ions, especially of ions from the Earth, although this precaution is somewhat academic in light of the strong autocorrelation of the *AE* index over many hours (see *Kamei and Maeda* [1981]; see also *Lennartsson and Shelley* [1986]).

The left and right panels of Figure 2 are based, respectively, on 2720 and 3804 independent density numbers, some of which fall below 10^{-3} cm^{-3}, even including some negative ones at beta $<10^{-2}$. Occasional negative "densities" are a normal statistical effect of subtracting a separately measured background count rate from the count rates in the various ion channels, when the signal-to-noise ratio falls below one. This is reflected in the bottom panels by large statistical uncertainties, or "errors," sometimes exceeding the density itself.

The errors plotted here are the ratio between the calculated standard deviation, which contains the background standard deviation twice (via a sum of variances; see *Lennartsson and Sharp* [1982]) and is positive by definition, and the absolute value of the net density. These numbers have been stored rounded to integers in the data files, representing a percentage, which accounts for the horizontal striations. Values of zero percent have been set to 0.5% when fitting the two straight lines (log-log scale) by the linear (unweighted) least squares method [*Bevington*, 1969, pp. 92–118]. These lines have no other purpose here but to highlight the inherent dependence of data quality on the local beta value. Needless to say, the corresponding correlation coefficients are significant, being $R = -0.77$ on the left and $= -0.79$ on the right [*Bevington*, 1969, pp. 119–127; *Press et al.*, 1986, pp. 484–487].

Figure 2 shows that a density of 10^{-3} cm^{-3} is typically close to the statistical limit of resolution of H^+ ions in these data. The reason is that density numbers used here, like other moments, are all based on essentially random measurements of the accessible velocity space, whether it is filled by mostly noise or mostly signal. It is possible to lower the sensitivity threshold another factor of 10, in terms of ion density, by concentrating on ions that are focused in energy and angle to within a few instrument accumulations [*Sharp*

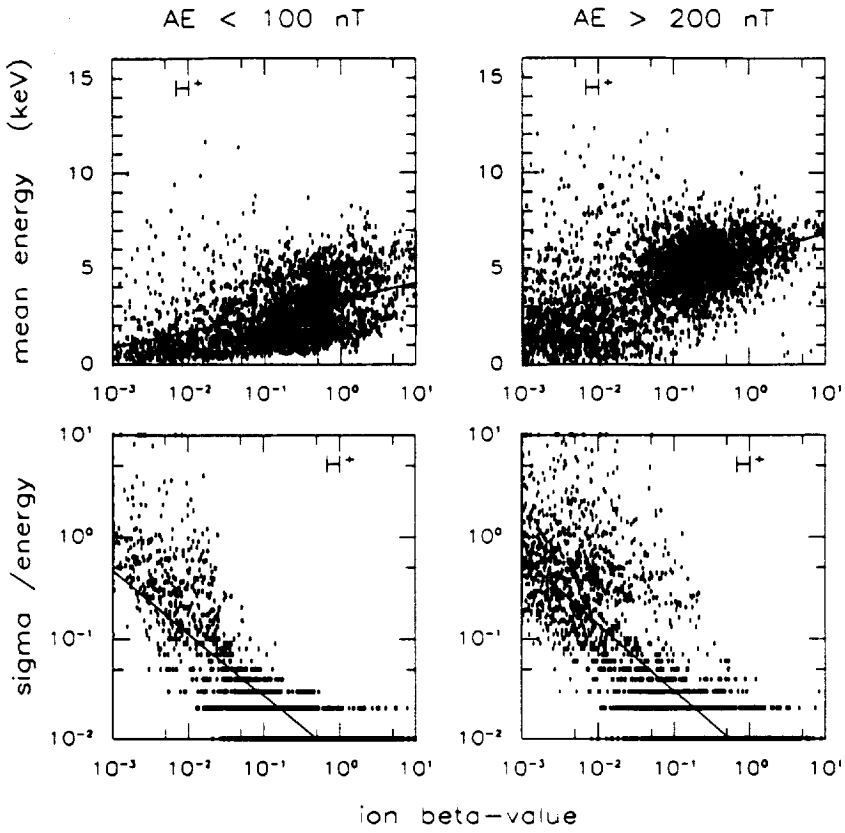

Figure 3. Corresponding (top) mean energies of H^+ ions and (bottom) their uncertainties.

et al., 1981], but that is also sure to exclude any hot and near-isotropic ion component that may be present.

To be more specific, an isotropic Maxwell-Boltzmann distribution of H^+ ions with a few keV thermal energy and a density of 10^{-3} cm^{-3} generates about one count every 2 to 4 s in this instrument, a rate roughly half as large as the typical background in the lobes, and a total of about 40 counts over the course of a full energy-angle scan of H^+ ions. That means 40 net counts after subtraction of an average background rate derived from a sum of 50 to 100 counts in the background channel (about the same total accumulation time). Hence it is practically impossible to discern such a distribution from an energy-angle spectrum of raw counts, but by subtracting an appropriate background and weighting and integrating the counts into number density it becomes possible, albeit with a standard deviation typically between 30% and 40%, because of the background standard deviation. This example illustrates the fact that the signal-to-noise ratio does not have to be greater than one in order for a calculated density to be greater than three standard deviations, but this ratio ought not to be much less than 1/2 with typical lobe background rates.

Figure 3 shows the H^+ mean energy (top) and relative uncertainty (bottom) in the same format, except that the top panels have a linear scale on the ordinate and linear regression lines as well ($R = 0.45$ on the left, $= 0.57$ on the right). Since the mean energy is a ratio between energy density and number density, it has no physical or mathematical meaning if either or both of those densities are negative, so energies have only been calculated for positive values of both densities. The resulting number of points is 2673 (left) and 3510 (right), and the regression lines in the bottom panels have $R = -0.84$ (left) and $= -0.85$ (right). It may be noted that energies, at any given beta, are typically higher at $AE > 200$ nT, while densities are lower (Figure 2).

Although the trend is clearly to have lower energies at lower beta, the very highest mean energies have also been sampled at beta <0.1. Except for a few, these extreme values are not, as one might expect, caused by large statistical errors, because most remain when these plots are redrawn including only values with a relative sigma of less than 1/3 (not shown). In some cases they appear to represent beams of H^+ ions moving toward the Earth at high speed (up to 1200 km s^{-1}; see also *DeCoster and Frank* [1979] and *Eastman et al.* [1985]), in other cases they may be the result of aliasing caused by brief enhancements in the ion flux while the instrument is sampling the higher-energy channels. The relative importance of rapid earthward flows may be judged from Figure 4, which shows the X component of the calculated bulk velocities of H^+ ions.

In any case the great majority of H^+ energies are quite low at low beta, especially at quiet times, a result that is consistent with many earlier reports of reduced proton energies adjacent to the tail lobes, as measured with regular electrostatic analyzers [e.g., *Akasofu et al.*, 1973]. Taken together, Figures 3 and 4 imply that the H^+ energies are generally dominated by random, or "thermal," motion at all beta. This will become even clearer when angular distributions are discussed in section 3.4. It should be mentioned that the regression lines in the top panels of Figure 3 remain almost identical when the plots are limited to points with sigma <1/3 (not shown). This is a good indicator that

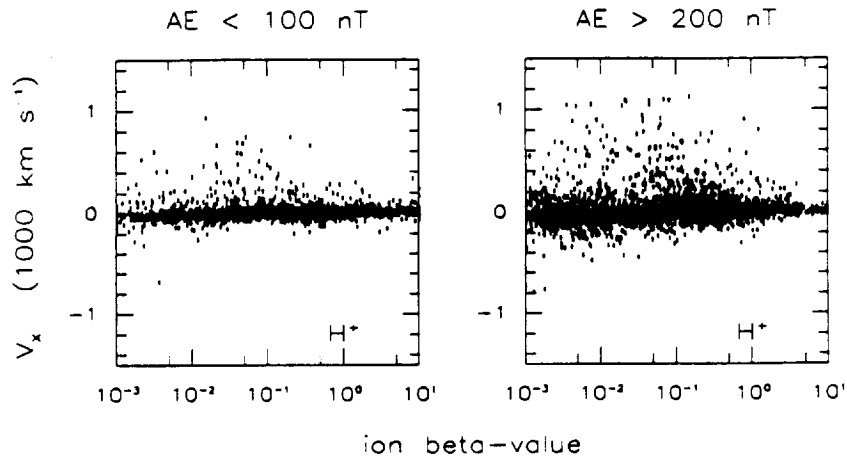

Figure 4. Corresponding drift velocity of H^+ ions along GSM (and GSE) X axis.

background counts have been properly subtracted from all samples, since the background would tend to bias the apparent mean energy toward a rather high value of about 5 keV/e.

3.2. Relative Densities of Other Ions

Figure 5 shows the ratios between the other ion densities and the H^+ density, as a function of the same beta and AE. In forming these ratios, each value of the H^+ density has first been compared with its own standard deviation, or sigma, and in the relatively rare events that it is smaller than one sigma (100% or greater error), including sign, the sigma value has been used to represent the H^+ density in each ratio. The reason for doing this is to avoid large but physically meaningless ratios.

The straight-line segments in each panel are least squares fits (log-log) to points at beta <0.1, only including positive ratios. Rather than enumerating the correlation coefficient and number of samplings for each panel, it may suffice to say that R is about −0.5 to −0.7 and is based on some 425 to 1374 samplings, which means that R is significant in each case. The feature of principal interest here is the consistent increase in the density ratios with decreasing beta. This implies that the H^+ density falls off faster than any of the other densities as one moves into a tail lobe from the plasma sheet.

There are numerous (hundreds of) negative ratios not shown in Figure 5, mostly at beta <0.1 (examples will be shown later). Negative densities are more common with He^{++}, He^+, and O^+ ions than with H^+ ions, for two reasons. One is that the heavier ions must have a larger number density in order to produce a given count rate at a given energy; the other is that the heavier ions generally have a lower count rate to begin with. The result is a lower signal-to-noise ratio and a greater sensitivity to background subtraction. This subject will be discussed in more detail below.

In order to verify the gross trends of the density ratios, Figure 6 shows a subset of the same data, one in which every ratio is based on densities, numerator as well as denominator, with a relative sigma of less than 1/3 (densities greater than 3 sigma). This subset is much smaller, especially at beta <0.01. Nevertheless, the six regression lines remain much the same in each case, and the respective correlation coefficients, ranging from a low of −0.34 (top left) to a high of −0.72 (middle left), are still significant, considering the remaining number of points. In fact, even in the least significant case, the one with the fewest points remaining (middle left; 43 points), the probability of having no actual correlation is less than 10^{-7} [*Bevington*, 1969, pp. 119–127; *Press et al.*, 1986, pp. 484–487].

It makes no difference whether the 3-sigma criterion used for Figure 6 is applied to the absolute value of each density, or only allows positive densities. At 3 sigma there are no negative ratios left, but there are still 3240 remaining positive ratios (adding all panels). Hence the problem with negative "densities" is eliminated at the 3-sigma level, in this case, although at that level a large portion of valid data is also being discarded. By comparison, there are still some 50 negative ratios left at the 2-sigma level (0.5% of all remaining values).

3.3. Intercomparison of Energies

Figure 7 is analogous to Figure 5, with mean energies substituted for densities. In Figure 7 the ratios have been formed without regard to standard deviations of either numerator or denominator. However, no negative values are involved here, since the mean energies, when calculated, are based on positive energy and number densities (see the explanation of H^+ energies above). The energies of He^{++}, He^+, and O^+ ions appear for the most part to be dominated by thermal motion, like those of the H^+ ions, but the statistics is frequently poor at low beta (see next section).

All ions, except the He^+, tend to become less energetic with decreasing beta, although the wide scatter in Figure 7 may seem to defy any trend. However, as the regression lines suggest, the He^{++} energy typically falls off at about the same rate as the H^+ energy (on a log-log scale), staying about 4 times higher than the H^+ energy, whereas the O^+ energy falls of slightly faster most of the time. The He^+ energy, for some reason, does not show this trend, so the He^+/H^+ energy ratio increases with decreasing beta.

Some of the scatter in Figure 7 is no doubt due to statistical errors, but much of it is real. As far as the He^+/H^+ and O^+/H^+ energy ratios are concerned, the large range of the scatter (two orders of magnitude) is probably real, since it remains about the same at the 3-sigma level, as do the regression lines (not shown). At that level of signifi-

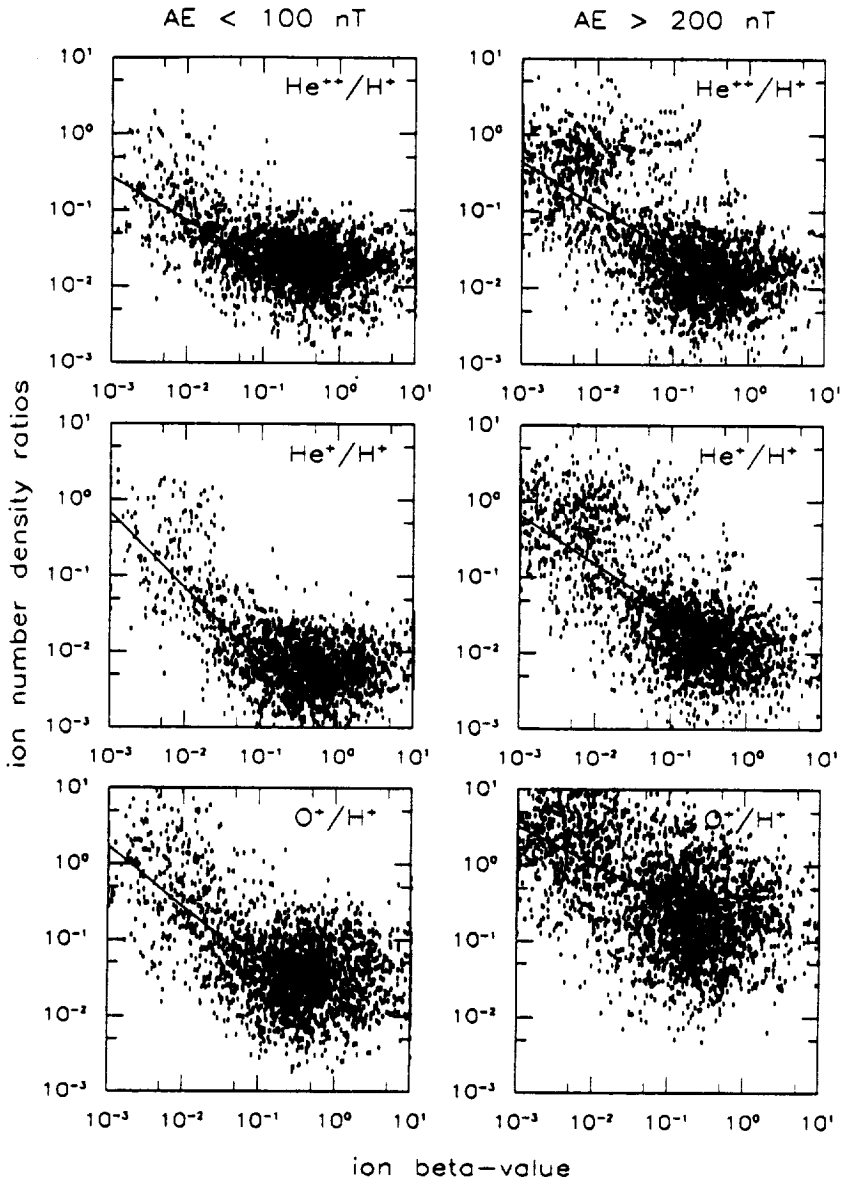

Figure 5. Densities of (top) He^{++}, (middle) He^{+}, and (bottom) O^{+}, normalized by the H^{+} density measured during same energy-mass scan cycle.

cance the He^{++}/H^{+} energy ratio is consistently greater than one and more strongly clustered near 4 (not shown).

Despite the scatter, the regression lines still have significant correlation coefficients, at least in the middle (R about -0.25; N about 2000 each) and bottom panels (R about 0.1; N about 2000 and 2700, respectively). The somewhat weaker correlation in the top panels (about -0.08) is of course consistent with a nearly flat regression line (at about 4).

3.4. Angular Distributions

Figure 8 compares the energies parallel and perpendicular to the tail magnetic field for each of H^{+}, He^{++}, and O^{+} ions under two conditions: (1) At least one of the two magnetic field directions has been sampled by the instrument field of view at all energies (extreme values of center pitch angle less than 5° or greater than 175°). (2) At least one of the two energies has been calculated with a relative sigma of less than 1/3.

The first condition gives a slight preference to ions flowing tailward along the field lines, because of the spacecraft orbit and the instrument configuration (see Figure 1 and section A1), but both field directions are commonly sampled during the same spin cycle, especially at energies below a few keV/e, where the field of view is rather wide (section A1). Of the two field directions, the tailward is favored by the O^{+} ions, especially at small beta (not shown), while the earthward is favored by He^{++} and H^{+} ions with flow speeds well in excess of 100 km s^{-1} (compare Figure 4).

The second condition prevents taking the ratio of two inaccurate numbers and thereby creating artificially large anisotropies. The main reason for not requiring a 3-sigma accuracy on both energies is to allow cases of extreme

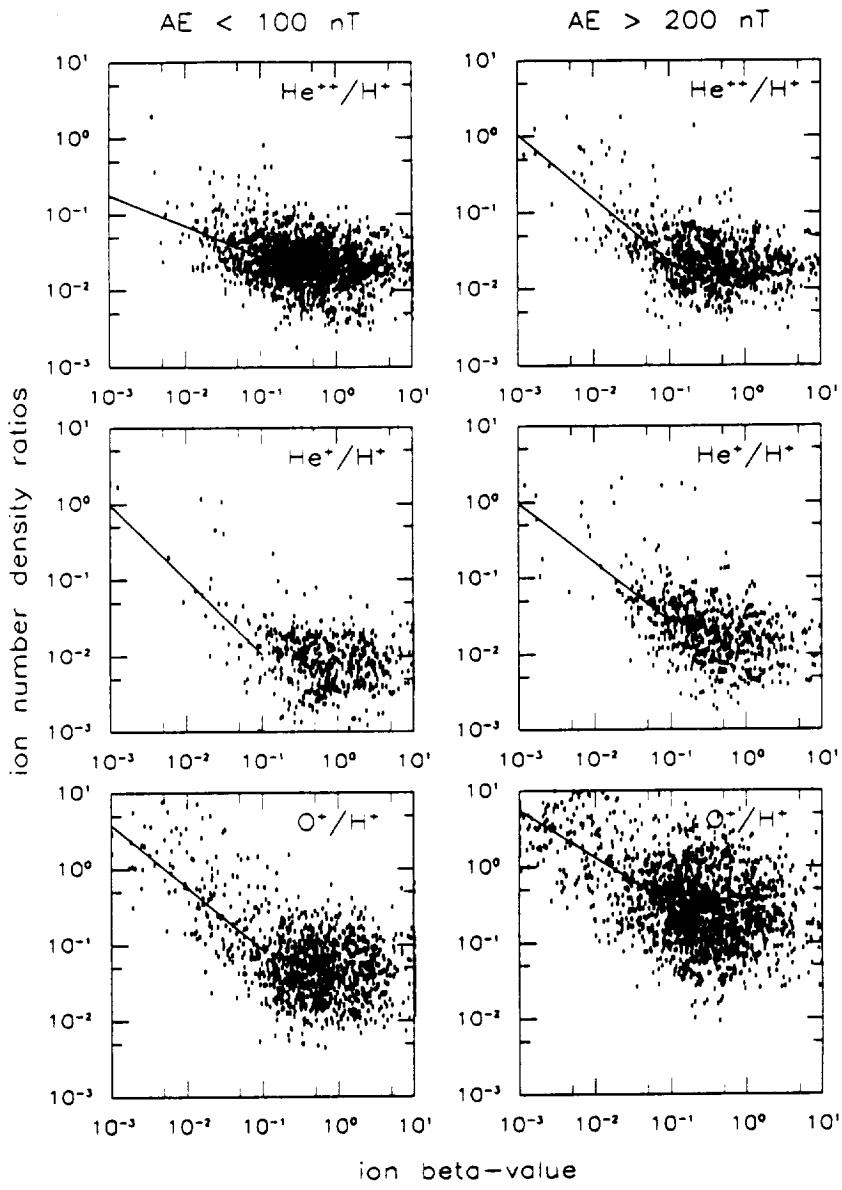

Figure 6. Same as Figure 5, but limited to measurements with less than 33% statistical uncertainty.

field-alignment, where the parallel flux contributes significant counts but the perpendicular flux may be buried in background noise. There is a barrier against very large such anisotropies, because of the 20° binning of the pitch angles during moment calculations (section A2). Even if all counts were confined to a single bin along either field direction, the center of the bin is either at 10° or 170°, so the ratio of parallel to perpendicular energy, when multiplied by two to adjust for the difference in degrees of freedom, could not exceed about 32, assuming no statistical errors in the background subtraction. However, few ratios even come close to 32 in Figure 8; the most common ratio is one, indicating a predominance of isotropic velocity distributions, at least for H^+ ions.

If the conditions on statistical accuracy are removed altogether, the main effects on Figure 8 are to increase both the number and spread of data points at small beta, especially for He^{++} and O^+ ions (about fivefold increase in number of points at beta <0.1 for O^+), as expected, but the regression lines remain very nearly the same (not shown). In other words, anisotropic ratios become more common, real or not, but they show no greater preference for either large or small values than already indicated in Figure 8. It may also be mentioned that He^+ ions, which are not part of Figure 8, have ratios similar to the O^+ ions, although they have fewer ratios with small sigmas.

A proper comparison of parallel and perpendicular energies should compensate for $\mathbf{E} \times \mathbf{B}$ drift. Since the latter is unknown here, the next best move is to determine the cross-B component of the measured ion drift velocity in the spacecraft spin plane (approximately the GSE X-Y plane), and subtract the corresponding drift energy from the perpendicular energy, so as to approximate pure gyrational (thermal) energy. In practice, this makes little difference, because the cross-B drift speed is generally small (mostly less than 50 km s^{-1}) compared to thermal velocities in these data.

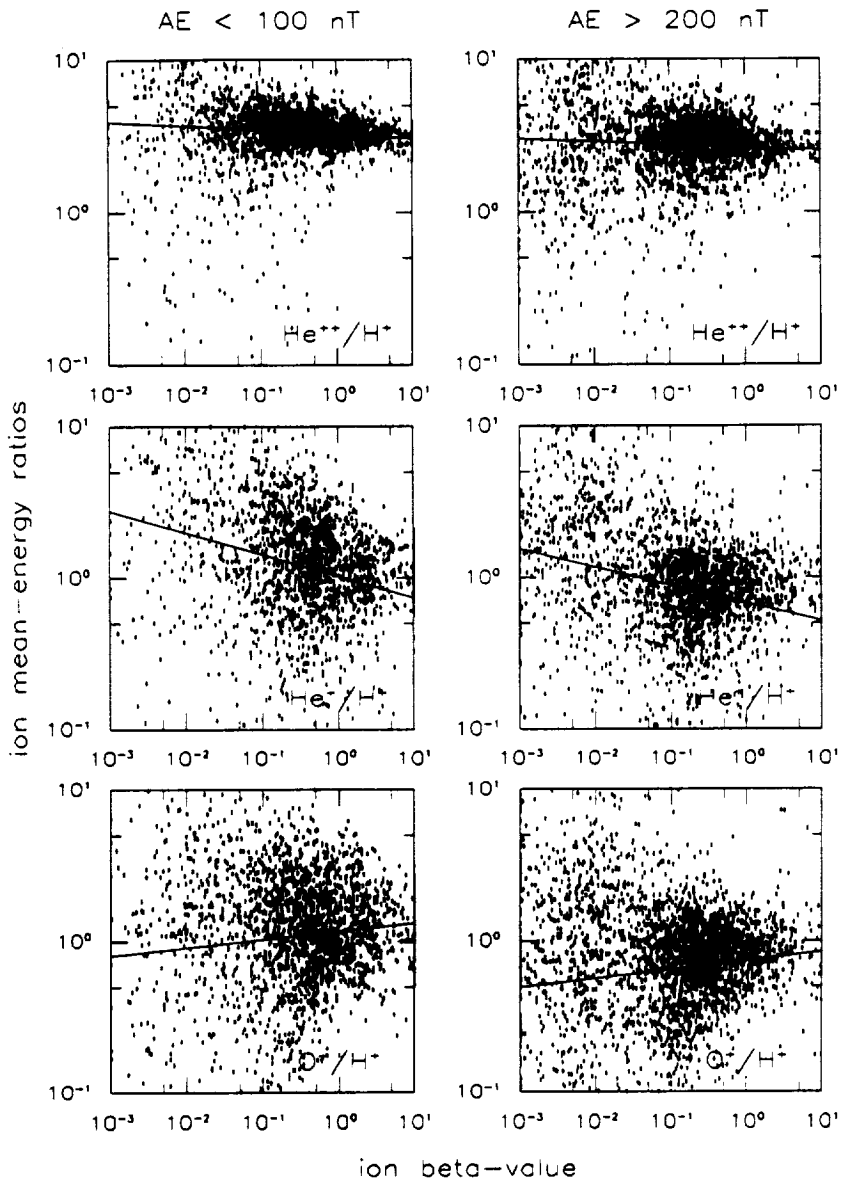

Figure 7. Mean energies of (top) He^{++}, (middle) He^{+}, and O^{+} (bottom), normalized by the H^{+} mean energy.

However, the ratios shown in Figure 8 have in fact all been "corrected" this way.

3.5. Extending the Energy Range Downward to 10 eV/*e*

The lowest-energy channel, from 10 eV/*e* to about 100 eV/*e*, not counting the variable RPA settings, has been sampled in about 90% of these data and is represented by a partial number density for each ion species, a quantity that may or may not be an accurate measure, depending on such unknowns as spacecraft potential and **E** × **B** drift direction and speed. This partial density can be added to the normal number density, and by weighting it with a suitable energy (40 eV/*e*) it can also be used to derive a modified value for the total mean energy.

Adding this low-end density has somewhat different effects at different beta, and the effects also vary with ion species. At beta >0.1, that is including the plasma sheet proper, the effects are consistently small, especially for H^{+} and He^{++} ions, whose density and energy are rarely changed by more than a few percent. The corresponding changes for He^{+} and O^{+} ions are somewhat larger, often reaching some 10 to 20%. At smaller beta, usually meaning smaller densities as well, the effects are much more variable, sometimes doubling or tripling the density, especially that of O^{+} ions. However, if Figures 2 through 8 are redrawn, including this energy channel whenever it has been sampled, the new figures (not shown) are difficult to distinguish from the old ones. There is some increase in the range of scatter, but very little change in the gross trends.

4. Discussion

The most intriguing result of this study is the variation of ion density ratios with beta in Figure 5, that is the increase at

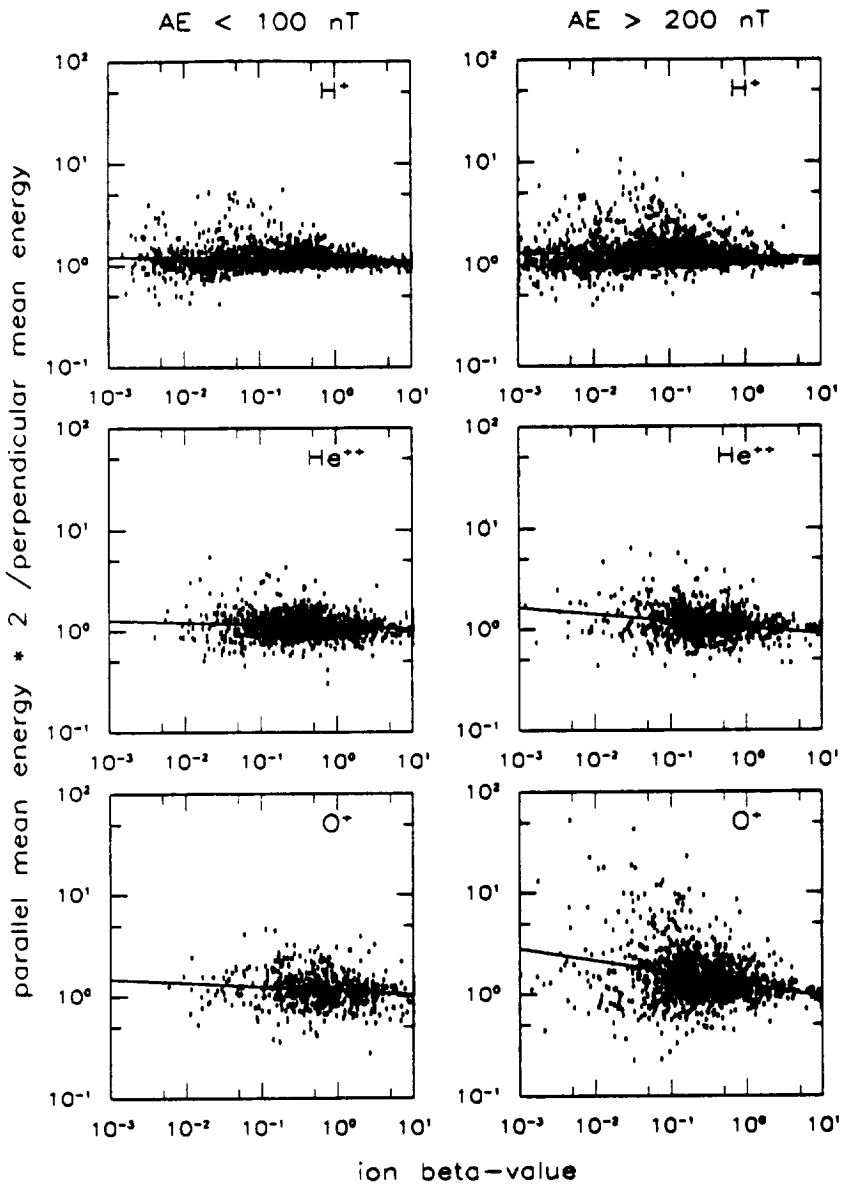

Figure 8. Parallel-to-perpendicular energy ratios for (top) H^+, (middle) He^{++}, and (bottom) O^+, when energies obtained with less than 33% statistical uncertainty (see text for details).

low beta. On one hand, it is in qualitative agreement with the theoretical result of *Kiessling and Ziegler* [1989] regarding the O^+/H^+ ratio, but on the other hand there are instrumental and statistical effects that will conspire to produce a similar result, as shown by the absolute values of negative ratios in Figure 9 (top panels). These effects are due to low count rates, low signal-to-noise ratio, and occasional time aliasing associated with the separate sampling of different ions and of ions and background. The data have been examined very extensively for evidence of these effects, both by imposing various selection criteria in the statistical analysis and by studying many sample events in detail. They are no doubt significant, as Figure 9 proves, but they do not appear to be the sole or even dominant reason.

Figure 10 illustrates some of the ambiguities inherent in low count rates and a low signal-to-noise ratio. Figure 10 actually represents one of the "better" events, in a formal sense, in that the signal-to-noise ratio is still greater than one, if only marginally, at the times when the He^{++}/H^+ ratio approaches unity. Even so, the low count rates make it fruitless to try to compare the ions in the raw data; it is necessary to sum counts into moments before any kind of pattern can be recognized. In this case the densities of H^+ and He^{++} ions become roughly comparable twice, when the H^+ density is at a local minimum (top panel).

This could still be a time aliasing effect in the background subtraction, since the background measured during the corresponding instrument cycles may have been lower than the actual background during the He^{++} samplings. However, by also comparing the mean energies of the two species in Figure 10, both on an E/Q (middle panel) and E/M basis (bottom panel), it appears that the data are at least consistent with a continuous signal for both H^+ and He^{++} ions. It is clear that the two sets of energies in this case are more

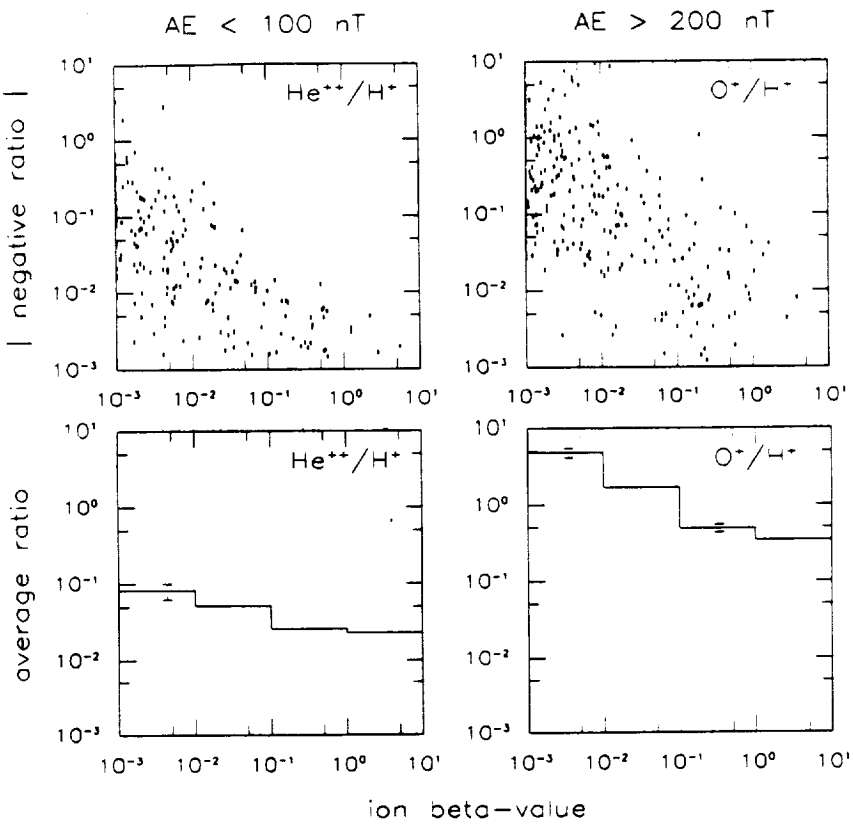

Figure 9. (Top) Examples of negative numbers (modulus) corresponding to the various panels of Figure 5. (Bottom) Corresponding averages (unweighted) when positive and negative numbers are both included (error bars indicate standard deviation of average when larger than line width).

nearly equal on an E/M basis. This would not be expected if background were dominant. In that case the energies would be widely scattered but have a tendency to show equal energy per charge on average, since the total range is measured in E/Q and only positive values are being calculated (the two species sometimes have equal mean E/Q even when their signals are far above background).

In some cases the He^{++}/H^+ ratio is significantly reduced when the energy range of the data is extended to include the 10- to 100-eV/e channel, but in general the inclusion of this channel only serves to increase the scatter, while the trends remain much the same, as already mentioned in section 3.5. It is worth noting that the H^+ ions in the 100-eV to 16-keV range usually have a mean energy of at least 500 eV even at low beta (Figure 3), and if these ions are part of a Maxwell-Boltzmann type distribution, their companions at energies below 100 eV have less than 20% of the total density. In those cases where a significantly larger H^+ density is present below 100 eV, that partial density is probably due to H^+ ions with a different history than the main population [cf. *Parks et al.*, 1992].

There are three principal reasons why the statistical trends in Figure 5 are probably real, at least qualitatively, even if many of the individual values are not. The first is that the trends in Figure 5 still survive in Figure 6, after all densities (numerator and denominator) with an absolute magnitude smaller than or equal to three sigmas have been discarded. The top and middle panels of Figure 6 have few points left at small beta, but the ones that do remain are consistent with the same kind of elevated ratios and cannot be easily ascribed to poor counting statistics. At this level of significance the background subtraction should be less critical, and that is confirmed by the elimination of negative ratios altogether, as mentioned above. In order for that to be an artifact, the formulas for density calculations would have to give lower weights to count rates from the background channel than they did to count rates from the ion channels, but those formulas do in fact give identical weight to both, except for the sign.

The second reason is that the same basic trends remain when the H^+ density is replaced by the "total" density from the energy-analysis section of the instrument (not shown). This density is calculated each time a mass-resolved density is produced (section A2), providing a continuous time reference that helps to eliminate time aliasing as a significant factor. There is only a minor reduction in the ratios using this replacement, consistent with the multiple-ion contribution to the total count rate (proportional to the square root of Q/M at a given energy).

The third reason is that those trends also emerge when the data are binned in beta and averaged within each bin, including all ratios, positive and negative. Two examples are shown in the bottom panels of Figure 9, the left one corresponding to the top left panel of Figure 5, the right one to the bottom right panel of Figure 5. These two examples essentially bracket the slopes of the average ratios corresponding to the other four panels of Figure 5 and are a strong indication that there is an underlying bias toward increased

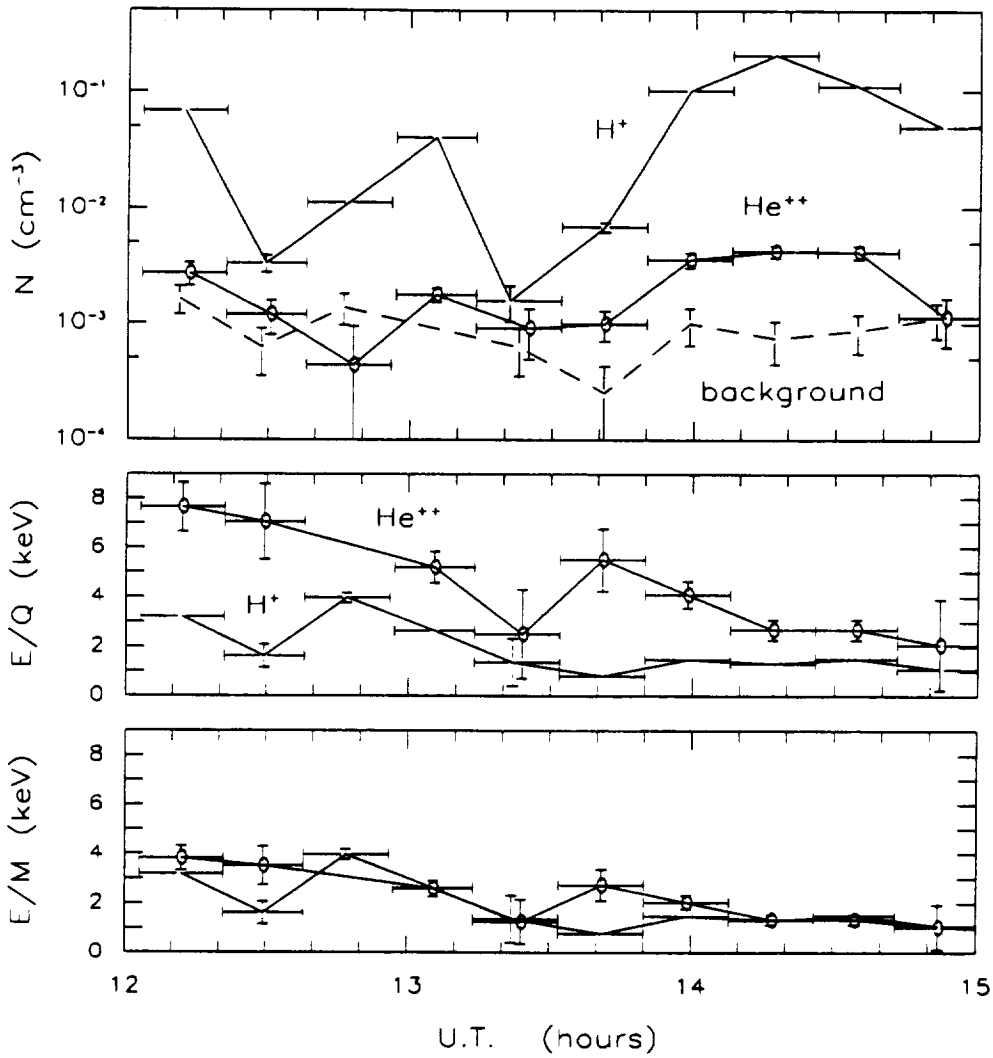

Figure 10. A 3-hour segment of data taken near local midnight on March 13, 1979, at 10 to 14R_E. Top panel shows densities of H^+ (line without symbols) and He^{++} (open circles), with background already subtracted, as well as the "density" of the background alone (dashed line) using weights corresponding to He^{++} ions. Lower panels show mean energies normalized by (middle) ionic charge or (bottom) mass. Horizontal bars indicate energy-mass scan cycle, vertical bars show standard deviation carried over from counting statistics.

positive ratios at low beta. This bias cannot be instrumental, because the detector response to penetrating radiation is independent of the M/Q setting of the optical parts and, as already stated, the formulas for density calculations would produce negative numbers as often as positive ones if count rates in the background channel and the ion channels were from the same statistical distribution.

Granted that there is a geophysical explanation for Figures 5 and 6, what specific physical quantity separates the different ions? One candidate might be the mean or median gyroradius of each species. At a geocentric distance $R > 10R_E$, and at beta <0.1 the tail magnetic field, as measured by the ISEE 1 magnetometer, typically ranges between 20 and 60 nT (depending mostly on distance from Earth). This means that a 3-keV H^+ ion, for example, has a gyroradius of 130 to 400 km at 90° pitch angle, and therefore a transverse range of 260 to 800 km during each gyration. This is small compared to the cross section of the tail, but not necessarily small compared to the transition region between the plasma sheet and tail lobes [e.g., *Parks et al.*, 1992, and references therein].

To make this point more tangible, assume the following: (1) Each density $n(i)$ of species i falls off with increasing distance dz from the plasma sheet proper with the functional dependence exp $(-dz/H)$, starting with $dz = 0$ at a point where beta = 0.1 (magnetic field already near its lobe value). (2) The "scale height" $H = H(i)$ is proportional to the mean gyroradius $g(i)$, and the proportionality constant is the same for all species. (3) The mean energy of each species is independent of dz, that is $H(i)$ is approximately constant. (4) Beta is dominated by the H^+ ions, which have the mean radius $g(H^+)$. Under these assumptions the coordinate dz can be approximated by

$$dz \approx H(H^+) \times \log [\text{beta}(0)/\text{beta}(dz)]/ \log (2.718)$$

and the ratio $r(i) = n(i)/n(H^+)$ is related to beta by

$$\log [r(i)] \approx A(i) - C(i) \times \log (\text{beta}) \quad (1)$$

where A and C are constants and

$$C(i) = [g(i) - g(H^+)]/g(i). \quad (2)$$

Considering that the gyroradius at a given pitch angle is proportional to the square root of the product of mass and energy and inversely proportional to charge, it would appear from the left panels of Figure 7 ($AE < 100$ nT), that the He^{++} ions should have a mean gyroradius twice that of H^+ ions (4 times the energy), assuming roughly isotropic velocity distributions (Figure 8), and the O^+ ions one that is about 4 times that of H^+ ions (about the same energy as the H^+). This means that the values of $C(i)$ for He^{++}/H^+ and O^+/H^+ in (2) ought to be about 1/2 and 3/4, respectively. Those numbers are in fact very close to the slopes of the respective regression lines in the left panels of Figure 5 (−0.56 and −0.80), a result that is surprising in view of the extreme simplicity of the assumptions.

Removing (3) and taking into account that the mean energies $E(i)$ of H^+, He^{++}, and O^+ ions decrease with decreasing beta, that is with increasing dz, means adding a third term $C(i) \times \log [E(H^+, dz)/E (H^+, 0)]$ on the right side of (1), but A and C are still constants as long as $E(i)/E (H^+)$ is constant. Inserting typical numbers for $E (H^+)$ from Figure 3 yields only small absolute values for this third term, at least an order of magnitude smaller than the second right-hand term in (1), so this equation is still a fair approximation, within the remaining assumptions, for the He^{++}/H^+ and O^+/H^+ ratios at $AE < 100$ nT.

On the other hand, (1) predicts that the He^+/H^+ ratio should have a slope intermediate between those of the He^{++}/H^+ and O^+/H^+ ratios, even after proper consideration of energies (A and C are not constant for He^+), while the left panels of Figure 5 (and Figure 6) show the steepest slope for the He^+/H^+ ratio. Furthermore, as beta receives greater contributions from ions other than the H^+ ions, especially from O^+ ions at active times, the slope of the log $[r(i)]$ versus log(beta) ought to increase, and that is not borne out in the right panels of Figure 5, so this simple "model" probably has severe limitations. All it really does is make it plausible that Figures 5 and 6 have a geophysical explanation. It should also be pointed out that the far more elaborate model of *Kiessling and Ziegler* [1989] does not have gyroradii as separate input parameters, although it does make the implicit assumption that the O^+ ions have four times larger gyroradii than the H^+ ions by assuming that both species have the same temperature (independent of beta).

5. Conclusions

To begin with, the large O^+/H^+ ratios in Figures 5 and 6 provide further evidence that ions of terrestrial origin constitute a large fraction of the tenuous energetic plasma in the tail lobes. This is keeping with the reasoning of *Sharp et al.* [1981], who based theirs on the large oxygen content of magnetic field-aligned ion streams. If one defines the lobes by beta <0.1 in these figures, it appears that during disturbed conditions ($AE > 200$ nT) the O^+ concentration typically exceeds that of H^+ ions, and is quite compatible with the finding by Sharp et al. that O^+ ions comprise about 2/3 to 3/4 of the tail lobe ion streams for $Kp > 3+$ (their Table 1). Since Figures 5 and 6 are based on all ion flux entering the instrument, not merely the peak flux, the large O^+ concentration measured here can be considered a generalization of the result of Sharp et al.

Where do H^+ ions fit in this picture? What is their principal origin? As far as their energies are concerned, they are much better correlated with the He^{++} ions than they are with either the O^+ or He^+ ions, according to Figure 7, which suggests that a majority of the H^+ ions in the Earth's tail are of solar rather than terrestrial origin, most of the time. This impression is strengthened by the observation that the H^+ and He^{++} ions tend to have about the same energy per nucleon in the top panels of Figure 7 (see specific example in Figure 10), a relationship that is characteristic of H^+ and He^{++} ions in the solar wind.

It should be mentioned that the slight negative slope of the He^{++}/H^+ regression lines in Figure 7 is probably an instrumental effect, caused by a combination of higher ion energies at higher beta (Figure 3) and the upper energy cutoff at 16 keV/e. Since the latter is measured in energy per charge, it leads to a more rapid loss of He^{++} than H^+ ions from the measured energy range if these ions are energized in proportion to either ionic mass or initial energy (see more extensive discussion of this subject by *Lennartsson and Shelley* [1986]). The same effect is probably responsible for the slight downward shift of the regression line at $AE > 200$ nT, since the H^+ and He^{++} energies are higher during active times (Figure 3).

Assuming that the H^+ ions are indeed mostly of solar origin, and ignoring for a moment the He^{++} ions, it follows from the bottom panels of Figures 5 and 6 that the solar ions usually outnumber the terrestrial ions in the plasma sheet, at beta >0.1. How do the solar ions reach the near-Earth plasma sheet? Do all of these ions arrive from the distant tail by the combined means of earthward jetting along the magnetic field lines and earthward convection in a predominantly dawn-dusk oriented electric field [e.g., *Speiser*, 1965], or do they enter in large part by cross-tail convection from the dawn and dusk flanks, as argued in *Lennartsson* [1992]? The answer to that question depends on the actual geometry and temporal behavior of the tail electric field, neither of which is well known at present. However, there are some features of these data that seem to favor the second means of transportation, that is the cross-tail convection.

As Figure 4 shows, it is easy to find rapid (hundreds of km s^{-1}) earthward flows of H^+ ions, especially during disturbed conditions ($AE > 200$ nT). However, these flows are not the normal state of motion of the H^+ ions, not even at low beta; the normal state is to have slow (tens of km s^{-1}) bulk motion, including both earthward and tailward components. If the H^+ ions were mostly arriving from the distant tail, say from $100R_E$ downtail [*Zwickl et al.*, 1984], moving along magnetic field lines while at the same time convecting into the plasma sheet, that is convecting toward higher beta, they would tend to disperse according to field-aligned speed, leaving the faster ions at the lower beta. There is really no evidence of that in Figure 4; faster and slower flows occur at the same beta, at least at beta <0.1, and the slower flows are dominant everywhere. This situation would seem to imply that the bulk of the H^+ ions must be able to reach the near-Earth plasma sheet from somewhere besides the distant tail, and one possible mode of access would be by inward

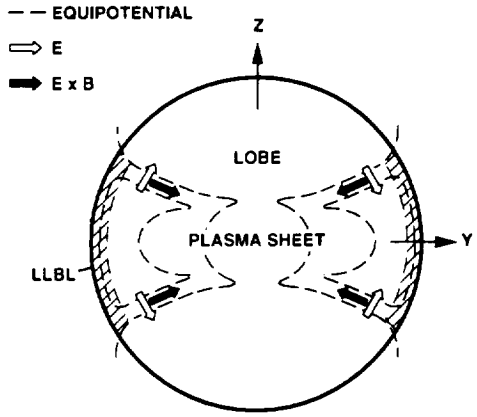

Figure 11. Hypothetical electric equipotentials (dashed lines) allowing inward tail convection from dawn and dusk flanks. These may originate in the low-latitude boundary layer (LLBL), as indicated by closed contours [*Lennartsson*, 1992], or in the solar wind, as indicated by open contours (assuming dawn-dusk directed E field in solar wind).

convection from the tail flanks, in an electric field that is locally north-south directed in a proper sense, for example as outlined in Figure 11.

It should be noted that the predominantly small V_X values at low beta in Figure 4 cannot be ascribed to poor counting statistics, since they cannot be consistently smaller than their absolute errors. Neither can they be ascribed to infrequent sampling of the earthward magnetic field-aligned direction, because the pitch angle range of the data is generally the widest at the lowest beta, and even when the data are limited to those with the most complete pitch angle coverage, as done in Figure 8, there is no significant field-aligned anisotropy in the H^+ population as a whole (top panels). So even though rapid earthward flows are common, a nearly isotropic velocity distribution is more common yet among H^+ ions at all beta. It is also worth mentioning that the particle counter in the energy-analysis section of the instrument does not detect a significantly more frequent occurrence of rapid earthward flows than does the "mass detector," even though its angular response is more favorable (in the northern lobe), counting ions moving in the spin plane or slightly downward (not shown).

Returning to the He^{++} ions, which may all be of solar origin, it should be mentioned that they have V_X values similar to those of the H^+ ions (not shown), including numerous negative ones (see examples in the work by *Lennartsson* [1992]), although the scatter is enhanced by frequently poor counting statistics. Of greater interest, however, is the difference between the He^{++} and H^+ ions in terms of their density gradients, as implied by Figures 5 and 6 (top panels). It is hard to imagine how this could arise from velocity dispersion among ions streaming earthward from the distant tail, since there is no indication that He^{++} ions are moving any faster than H^+ ions in general (about same E/M in Figure 7). Furthermore, this spatial relationship between the He^{++} and H^+ ions is basically similar to the relationship between the O^+ and H^+ ions, even though the O^+ ions are flowing almost exclusively tailward at low beta (not shown) and have generally small velocities as well (fairly low energies in Figure 7 despite the large ionic mass).

As suggested by the simple exercise in the preceding section, the varying density gradients may be physically related to the different gyroradii of different ions. If that is true, it would seem to require that the gyrocenter motion of all ions is largely perpendicular to the density gradients, that is parallel to the boundary between the plasma sheet and the lobes. That state of motion could be set up in accordance with Figure 11, for example.

Since the mass-dependent gradients in Figures 5 and 6 are qualitatively similar to the theoretical result of *Kiessling and Ziegler* [1989] for H^+ and O^+ ions, whether or not the ion gyroradii are truly the ordering parameters, it is reasonable to assume that there may also be some fundamental similarities between actual and modeled particle drifts. It is therefore interesting to note that their model, which has only two spatial coordinates, GSM X and Z, assumes purely one-dimensional bulk motion along the Y axis, that is along surfaces of constant magnetic field and constant beta. Despite the two-dimensional character of their model, that state of motion is conceptually similar to having ions convect according to Figure 11.

The obvious test to make with the existing data is to examine how the calculated bulk velocities in the GSE Y direction vary across the tail. A preliminary study along those lines has been made, using the ion beta as a measure of latitude, but the results are not yet conclusive. The calculated V_Y values are typically in the range of tens of km s^{-1}, and are to some extent consistent with Figure 11 (not shown), but it appears that beta is inadequate as a measure of location across the shear boundary in the velocity field, and further study is required. In order to extract true bulk velocities it is also necessary to consider the effects of a gradient in the spatial distribution of ion gyrational motion (due to the density gradients).

Finally, it is natural to view Figures 5 and 6 against the now well-documented "deficiency" in the magnetospheric content of He^{++} ions when compared to the solar wind [e.g., *Young et al.*, 1982; *Gloeckler and Hamilton*, 1987]. The central plasma sheet was found to have a higher He^{++}/H^+ ratio than the inner magnetosphere by *Lennartsson and Shelley* [1986], reaching average values of about 3% during quiet conditions, but still lower than the typical solar wind ratio of about 4% during the same phase of the solar cycle (rising phase; see for example *Feldman et al.* [1978]). According to Figures 5 and 6, the He^{++}/H^+ ratio is instead enhanced over solar wind values in the tail lobes. Does this mean that solar wind He^{++} ions are partially stripped away from the accompanying H^+ ions during entry into the geotail and subsequently left behind in the lobes? This scenario cannot be excluded at this point, but if Figure 11 properly depicts the plasma convection, then the He^{++} ions would eventually rejoin the H^+ ions when the convection turns into the central plasma sheet. Another possible explanation for the reduced He^{++}/H^+ ratio in the central plasma sheet (and inner magnetosphere) is of course the admixture of terrestrial H^+ ions. Being that the H^+ and He^{++} ions often have about equal velocity distribution in the tail (Figure 7), this admixture may start at an early stage of solar plasma entry, for example in the cusp regions, as perhaps suggested by the numerical modeling of *Delcourt et al.* [1989].

Appendix

A1. Instrumentation

The ISEE 1 spacecraft (along with the ISEE 2) was launched on October 22, 1977, into an orbit with apogee at almost $23R_E$ (geocentric), perigee at about 300 km altitude, an inclination of 29°, and an orbital period of 57 hours. It was placed in a spinning mode with the axis nearly perpendicular to the solar ecliptic plane and with a period of approximately 3 s.

The Lockheed ion composition experiment on the ISEE 1 is one of a family of instruments using the same type of ion optics and covering nearly the same range of energies (0 eV/*e* to about 17 keV/*e*) which have also been flown on GEOS 1 and 2, DE 1, and AMPTE/CCE [*Shelley et al.*, 1978]. The ISEE 1 instrument consists of two nearly identical mass spectrometers with the respective fields of view centered 5° above and 5° below the spin plane, that is about 5° above and below the solar ecliptic plane. Data used in this study are from one of these, the one looking below the spin plane (seeing ions moving upward). Each field of view is about 10° wide along the spin plane, and some 10° to 50° wide transverse to this plane, being the widest at the low energy end (due to preacceleration) and gradually decreasing toward 10° with increasing energy. Information on the instantaneous pitch angles (at center of field of view) is provided by the ISEE 1 flux gate magnetometer [*Russell*, 1978].

Each spectrometer consists of an electrostatic analyzer to select energy per charge, followed by a combined electrostatic and magnetic analyzer to select mass per charge. Both analyzer sections have particle detectors, so at each energy setting the experiment provides both the total ion flux and the partial flux at a selected mass per charge. On ISEE 1 each combination of energy and mass is maintained for at least 1/16 s in high telemetry bit rate and 1/4 s in low (normal) bit rate. Different combinations are stepped through in a cyclic fashion according to patterns controlled by a random access memory which is programmable from the ground. The various ISEE 1 patterns, or "modes," used inside the magnetosphere require anywhere from 2 to 20 min to complete. The mass selections usually include one that blocks all ions from reaching the second detector, allowing intermittent measurements during each cycle of the noise associated with penetrating radiation. These measurements are later used to correct the count rates of mass analyzed ions. The total count rate in the first detector is not corrected this way, but this detector is much less susceptible to penetrating radiation because of its small size (spiraltron).

The maximum energy range of the ISEE 1 instrument is 0 eV/*e* (or spacecraft potential) to 17.9 keV/*e*, divided into 32 contiguous channels, although only a subset of these may be used in a given mode. The lowest channel, from 0 eV/*e* to about 100 eV/*e*, is normally limited to energies above 10 eV/*e* by a retarding potential analyzer (RPA) in the entrance. That same RPA is used to provide "cold plasma" data from 0 to 100 eV/*e* (retarding within the lowest channel) during parts of some scan cycles. Because of measurement uncertainties associated with spacecraft charging and plasma convection, the lowest-energy channel is treated separately when calculating velocity moments. Data from the highest-energy channel (above 16 keV/*e*) are excluded altogether here, because of a slight variation over time of the mass response of the ISEE 1 instrument in that channel. The numerical procedures used for weighting and summing counts from the various energy channels are such that the velocity moments correspond to an energy range of either 100 eV/*e* to 16 keV/*e* (in all figures) or 10 to 100 eV/*e* (discussed separately), the latter assuming no spacecraft charging.

The data used here have been obtained in several different energy-mass scan modes, but only in modes spanning at least the 0.1- to 16-keV/*e* energy range, whether that range is covered in a contiguous fashion (normally true) or not (see below), and only in modes which provide H^+ data from the mass analyzer, as opposed to modes which rely on "total ion" counts for approximate H^+ measurements. Any sampling that has not been corrected for background noise, because of gaps in the telemetry, for example, has been discarded.

A2. Data Format

This study makes use of an archival data set recently completed for NASA's Explorer Project and placed in the NSSDC under index number 77-102A-12I. The format of these data is designed to be a compact representation with roughly the same time resolution as that provided by the instrument energy-mass scan cycle. Although these data include various spectral information, this study is mainly based on files which contain velocity moments. Only a brief outline of the format can be provided here; a detailed explanation (user guide) may be obtained from the NSSDC. The time coverage of these data spans the so called "prime period" of ISEE operations, from the time of launch of ISEE 1 and 2 through the end of February 1980.

The main type of file used here contains separate velocity moments for the four principal ion species, H^+, He^{++}, He^+, and O^+, or in some cases a subset of these ions, depending on the instrument operating mode. The moments have been calculated once each energy-mass scan cycle, using two different methods to be explained below. In cases where the energy scans have left some channels unsampled, sometimes every other channel, an interpolation procedure has been employed, essentially assuming a linear variation of the differential flux. Each moment has a statistical uncertainty (standard deviation) assigned to it, calculated with standard formulas for error propagation [e.g., *Bevington*, 1969, pp. 56–64] assuming Poisson counting statistics and including the uncertainty in background subtraction [*Lennartsson and Sharp*, 1982].

A second type of file has velocity moments for "total ions," based on the total ion count rate in the electrostatic analyzer and assuming that this rate is due entirely to H^+ ions. These moments have been calculated once per energy scan, providing a time resolution of a couple of minutes or better, and usually have nearly continuous time coverage. The reason for using "total" moments here is to help interpret the mass-resolved moments (see text).

To calculate full three-dimensional velocity moments from the raw ISEE 1 data, the ion fluxes measured within the near-ecliptic field of view have been extrapolated to other angles using either of two sets of approximating assumptions:

1. The principal ion flow is parallel to the solar ecliptic plane and the ion fluxes have rotational symmetry around the flow vector, regardless of the magnetic field orientation. The direction of the flow vector within this plane is deter-